

## Role of strain in magnetotransport properties of Pr<sub>0.67</sub>Sr<sub>0.33</sub>MnO<sub>3</sub> thin films

H. S. Wang, E. Wertz, Y. F. Hu, Qi Li, and D. G. Schlom

Citation: *Journal of Applied Physics* **87**, 7409 (2000); doi: 10.1063/1.373002

View online: <http://dx.doi.org/10.1063/1.373002>

View Table of Contents: <http://scitation.aip.org/content/aip/journal/jap/87/10?ver=pdfcov>

Published by the [AIP Publishing](#)

### Articles you may be interested in

Three-dimensional strain state and spacer thickness-dependent properties of epitaxial Pr<sub>0.7</sub>Sr<sub>0.3</sub>MnO<sub>3</sub>/La<sub>0.5</sub>Ca<sub>0.5</sub>MnO<sub>3</sub>/Pr<sub>0.7</sub>Sr<sub>0.3</sub>MnO<sub>3</sub> trilayer structure

*J. Appl. Phys.* **115**, 233911 (2014); 10.1063/1.4884995

Effect of substrate-induced strain on transport and magnetic properties of epitaxial La<sub>0.66</sub>Sr<sub>0.33</sub>MnO<sub>3</sub> thin films

*Appl. Phys. Lett.* **91**, 012511 (2007); 10.1063/1.2750399

Substrate induced strain effects in epitaxial La<sub>0.67-x</sub>Pr<sub>x</sub>Ca<sub>0.33</sub>MnO<sub>3</sub> thin films

*J. Appl. Phys.* **93**, 5507 (2003); 10.1063/1.1566090

Suppression of structural and magnetotransport transitions in compressed Pr<sub>0.5</sub>Sr<sub>0.5</sub>MnO<sub>3</sub> thin films resulting in colossal magnetoresistance effect

*Appl. Phys. Lett.* **78**, 3857 (2001); 10.1063/1.1379592

Strain-dependent magnetic phase diagram of epitaxial La<sub>0.67</sub>Sr<sub>0.33</sub>MnO<sub>3</sub> thin films

*Appl. Phys. Lett.* **76**, 2421 (2000); 10.1063/1.126363

The new SR865 *2 MHz Lock-In Amplifier ... \$7950*



**Chart recording**      **FFT displays**      **Trend analysis**

**Features**

- Intuitive front-panel operation
- Touchscreen data display
- Save data & screen shots to USB flash drive
- Embedded web server and iOS app
- Synch multiple SR865s via 10 MHz timebase I/O
- View results on a TV or monitor (HDMI output)

**Specs**

- 1 mHz to 2 MHz
- 2.5 nV/√Hz input noise
- 1 μs to 30 ks time constants
- 1.25 MHz data streaming rate
- Sine out with DC offset
- GPIB, RS-232, Ethernet & USB

**SRS Stanford Research Systems**  
www.thinkSRS.com · Tel: (408)744-9040

# Role of strain in magnetotransport properties of $\text{Pr}_{0.67}\text{Sr}_{0.33}\text{MnO}_3$ thin films

H. S. Wang,<sup>a)</sup> E. Wertz, Y. F. Hu, and Qi Li

*Department of Physics, Pennsylvania State University, University Park, Pennsylvania 16802*

D. G. Schlom

*Department of Materials Science and Engineering, Pennsylvania State University, University Park, Pennsylvania 16802-5005*

(Received 18 August 1999; accepted for publication 28 January 2000)

We have studied the strain effects on the structural and magnetotransport properties of  $\text{Pr}_{0.67}\text{Sr}_{0.33}\text{MnO}_3$  (PSMO) thin films. The PSMO films were epitaxially grown on  $\text{LaAlO}_3$  (001),  $\text{SrTiO}_3$  (001), and  $\text{NdGaO}_3$  (110) substrates that induce biaxial compressive, tensile, and almost no strain in the films, respectively. The film thickness  $t$ , varied between 4–400 nm, was used as another controlling parameter of strain for each type of film. There exist two distinct thickness ranges with different thickness dependence of the magnetotransport properties. For  $t < 20$  nm, the zero-field resistance peak temperature ( $T_p$ ) and the high-field magnetoresistance (HFMR) properties are critically dependent on the thickness and the substrate. For  $t > 20$  nm, the  $T_p$  and the HFMR ratio show weak  $t$  dependence. The results show evidence for the effects of the Jahn–Teller type distortion as well as disorders on the resistive transition temperature and the HFMR. © 2000 American Institute of Physics. [S0021-8979(00)06909-7]

## I. INTRODUCTION

The discovery of the colossal magnetoresistance (CMR)<sup>1</sup> in the perovskite manganites  $\text{R}_{1-x}\text{A}_x\text{MnO}_3$ , where R and A are rare-earth and alkaline-earth elements, respectively, has invigorated renewed interest in these compounds. One fundamental question regarding the physical mechanism of the CMR property is whether the well established double-exchange (DE)<sup>2</sup> theory is sufficient to interpret the CMR effect in these materials. Theoretical analysis based on the Jahn–Teller (J–T) effect proposed by Millis *et al.*<sup>3</sup> and others<sup>4</sup> suggests that a strong electron–phonon interaction must be considered in any explanation of the magnetotransport properties of the CMR materials. High pressure<sup>5</sup> and neutron diffraction<sup>6</sup> experiments on bulk CMR materials have provided evidence for the J–T effect in the system. Since uniaxial lattice distortion can be easily introduced in thin films due to the lattice mismatch between the film and the substrate, it has been suggested that thin film samples are good candidates for studying the effect of lattice distortion, particularly the J–T type distortion,<sup>3</sup> on the electrical and magnetic properties of the manganites.

Recently, several groups have reported strain effects on the transition temperature and the magnetoresistance (MR) of manganite thin films,<sup>7–9</sup> but the results are often not consistent with each other. Millis *et al.*<sup>7</sup> studied the thickness dependence of the Curie temperature  $T_C$  in  $\text{La}_{0.7}\text{Ca}_{0.3}\text{MnO}_3$  (LCMO) films grown on  $\text{LaAlO}_3$  (001) substrates. They obtained a monotonic reduction of  $T_C$  when the film thickness decreases and attributed it to a J–T term of the lattice distortion. However, Rao *et al.*<sup>8</sup> did not observe any connection between the change of  $T_C$  and the J–T effect. Jin *et al.*<sup>9</sup> found that the MR is maximum when the film thickness is

about 10 nm which cannot be explained by the strain effect. Therefore, a systematic investigation of the CMR films with well-controlled strain is needed in order to better understand the role of strain in CMR materials.

In this work, we report a study of magnetotransport properties of  $\text{Pr}_{0.67}\text{Sr}_{0.33}\text{MnO}_3$  (PSMO) films grown on three different types of substrates with thickness in the range of 4–400 nm. The substrates are  $\text{LaAlO}_3$  (001) (LAO),  $\text{SrTiO}_3$  (001) (STO), and  $\text{NdGaO}_3$  (110) (NGO), which can induce biaxial compressive, tensile, and very little strain in the PSMO films, respectively. Measurements on the lattice parameters, the resistive transition temperatures,  $T_p$ , the low-field MR (LFMR), and the high-field MR (HFMR) were conducted. We have found that these properties depend strongly on the film thickness,  $t$ , in the strained samples and there are two different thickness regions that show different thickness dependences of  $T_p$ , LFMR, and HFMR. For  $t < 20$  nm, the  $T_p$  drops and the LFMR and HFMR increase sharply when the thickness decreases. For  $t > 20$  nm,  $T_p$ , LFMR, and HFMR all change only slightly with the film thickness. Moreover, the tensile-strained PSMO/STO films have lower  $T_p$  and stronger thickness dependence than the compressive-strained PSMO/LAO films. These results show that different strains all affect the magnetotransport properties in PSMO films and the effects on  $T_p$  and HFMR can be partially explained by the J–T type distortions and disorder effects.

## II. EXPERIMENT

The PSMO films were epitaxially grown on LAO, STO, and NGO substrates by pulsed laser deposition.<sup>10,11</sup> A ceramic PSMO disk with nominal composition of  $\text{Pr}_{0.67}\text{Sr}_{0.33}\text{MnO}_3$  was used as the target. An excimer laser with a wavelength of 248 nm, energy density of  $\sim 2$  J/cm<sup>2</sup>, and repetition rate of 5 Hz were used. The growth rate was

<sup>a)</sup>Electronic mail: hwang@phys.psu.edu

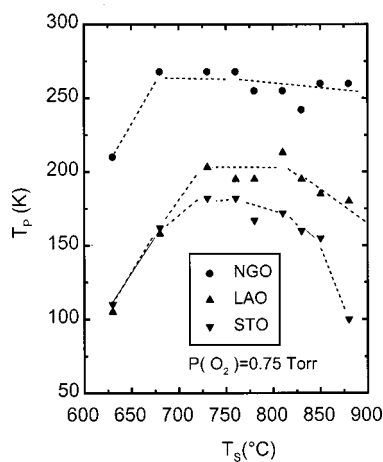


FIG. 1. Substrate temperature dependence of the  $T_p$  of the PSMO films on LAO ( $\blacktriangle$ ), NGO ( $\bullet$ ), and STO ( $\blacktriangledown$ ) substrates, respectively.

0.5–1 Å/s. In order to optimize the growth conditions for each substrate, we have studied the dependence of the peak resistivity,  $\rho_p$ , and the  $T_p$  on the substrate temperature ( $T_s$ ) and oxygen pressure during deposition. We found that in the pressure range of 0.5–0.8 Torr,  $\rho_p$  and  $T_p$  are not sensitive to the oxygen pressure and the  $T_p$  of the thick films is close to that of the target material. Therefore, for this study, we have chosen an oxygen pressure of 0.75 Torr for the deposition. Shown in Fig. 1 is the dependence of  $T_p$  on  $T_s$  for a series of 20 nm thick PSMO films prepared on different substrates. As seen in the figure, we can achieve the optimum  $T_p$  value for each substrate in a relatively wide range of  $T_s$ . The optimum  $T_p$  values are different for films on different substrates, which will be discussed later in the article. For NGO substrates, the  $T_p$  is almost constant for  $T_s$  between 670 and 880 °C. For LAO and STO substrates, the temperature window for optimum  $T_p$  is between 730 and 800 °C, which is narrower than that for the NGO substrate. The optimum  $T_s$  appears to be similar for all the substrates. Therefore, for the films studied in this work, we have chosen the same  $T_s$  at 780 °C for all the substrates. After deposition, the films were cooled down to room temperature in one atmosphere oxygen.

X-ray diffraction (XRD)  $\theta$ – $2\theta$ ,  $\phi$ , and  $\omega$  scans were used to examine the phase purity, crystallographic perfection, orientation relationship, and lattice constants of the PSMO films. The scans were performed with a Picker four-circle diffractometer using a Cu  $K\alpha$  radiation. The magnetoresistance was measured using a Quantum Design PPMS 6000 system with a standard four-terminal method. The magnetic field was applied perpendicular to the film plane.

### III. STRUCTURES

The doped bulk manganite PSMO ( $x=0.3$ ) is a distorted perovskite with a pseudocubic lattice parameter  $a_b=3.867$  Å.<sup>12</sup> The lattice mismatch between the PSMO film and the NGO (110) substrate ( $a\sim 3.86$  Å) at room temperature is only  $\sim 0.3\%$ , and therefore the PSMO/NGO films are expected to have little lattice mismatch induced strain. The pseudocubic LAO substrate has a smaller (3.79 Å), and the cubic STO has a larger (3.905 Å) lattice constant than the

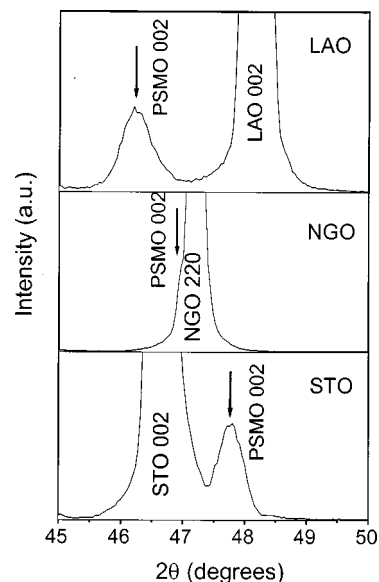


FIG. 2. XRD patterns of three 30 nm thick PSMO films grown on LAO, NGO, and STO substrates, respectively. The arrows indicate the PSMO 002 peaks.

PSMO at room temperature, and hence the PSMO/LAO films are compressed biaxially and the PSMO/STO films are expanded biaxially in the film plane. Correspondingly, the lattice parameters in the film normal axis are expected to expand in the PSMO/LAO films and to compress in the PSMO/STO films. Therefore, the lattice constants of the three types of films will show different thickness dependence.

The XRD experiments show that all the PSMO films are grown epitaxially with the  $c$  axes normal to the film plane. No impurity phases were found. Shown in Fig. 2 are XRD  $\vartheta$ – $2\vartheta$  scans near the 002 peak of PSMO for three 30 nm thick films grown on LAO, NGO, and STO substrates, respectively. As indicated in the figure, the 002 peaks of the PSMO/LAO and PSMO/STO films are located at  $46.2^\circ$  and  $47.8^\circ$ , corresponding to  $c$  axis lattice parameters of 3.93 and 3.81 Å, respectively. Note that although PSMO is pseudocubic in bulk, heteroepitaxial PSMO thin films are tetragonally distorted due to biaxial in-plane strain. We refer to the out-of-plane lattice parameter as  $c$  and the in-plane lattice parameter as  $a_f$ . The diffraction peak of the PSMO/NGO film is almost indistinguishable from the substrate peak due to their close lattice match. The peak positions of the PSMO/LAO and PSMO/STO films vary with film thickness. With the thickness decreases, the diffraction peaks become broader and their intensity is reduced, especially for the highly strained films. As shown in Fig. 3, the XRD  $\phi$ -scan shows sharp peaks and almost equal peak intensity, indicating high quality in-plane epitaxy and the expected cube-on-cube alignment of the unit cell of the perovskite film with the underlying substrate. These features have been found in films with thickness ranging from 7.5 to 400 nm.

The  $c$  axis lattice parameter as a function of film thickness is shown in Fig. 4. As expected, the  $c$  value of the PSMO/NGO films is almost independent of  $t$ , while those of the PSMO/LAO and PSMO/STO films are strongly depen-

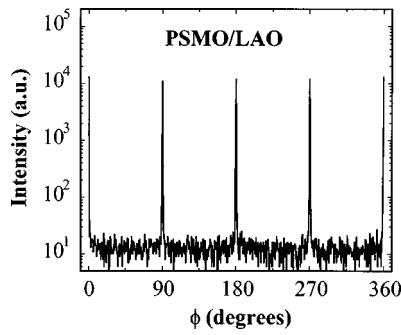


FIG. 3. X-ray  $\phi$ -scan of the 220 peak of a 150 nm PSMO/LAO film.  $\phi=0^\circ$  was set along the LAO [100] direction. The four peaks indicate that the PSMO film is epitaxial with an in-plane orientation relationship of PSMO [100]||LAO[100], i.e., cube-on-cube. The in-plane lattice constant of the PSMO is  $a_f=3.82\pm 0.02$  Å.

dent on  $t$ . When  $t$  increases from a few nanometers to above 250 nm, the  $c$  value of the PSMO/LAO films decreases from about 3.95 to 3.87 Å, while that of the PSMO/STO films increases from 3.80 to 3.84 Å. Figure 4 clearly indicates that the crystal lattice of the PSMO film in the  $c$  direction is expanded for the compressive-strain films and contracted for the tensile-strain films. The strain is gradually relieved with increasing film thickness when  $t$  is larger than about 20 nm and the  $c$  value gradually approaches that of the bulk PSMO crystal (3.867 Å).<sup>12</sup> We are unable to measure the in-plane lattice parameters for all the samples. From the samples we measured, we found that for 10 nm thick samples, the PSMO/STO film is fully strained with  $a_f=3.90$  Å and the PSMO/LAO film is partially strained with  $a_f=3.81$  Å.

Besides the lattice mismatch between the film and the substrate, the difference in the thermal expansion between the film and the substrate materials may also contribute to the measured lattice distortion of the films. Unfortunately, the thermal expansion coefficient of PSMO is not available, and therefore it is difficult to estimate the effect on the lattice parameters of the films. Nevertheless, given the fact that the thermal expansions of LAO ( $1\times 10^{-5}$  K<sup>-1</sup>), STO ( $0.9\times 10^{-5}$  K<sup>-1</sup>), and NGO ( $1.1\times 10^{-5}$  K<sup>-1</sup>) are very close to each other, the thermal expansion contribution to the lattice distortions should be similar for the three types of films.

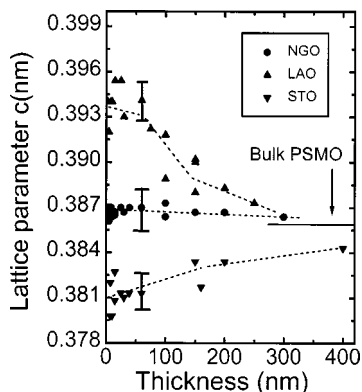


FIG. 4. Thickness dependence of the  $c$  axis lattice parameters of the PSMO films grown on LAO ( $\blacktriangle$ ), NGO ( $\bullet$ ), and STO ( $\blacktriangledown$ ) substrates, respectively. Dashed lines are guide to the eyes.

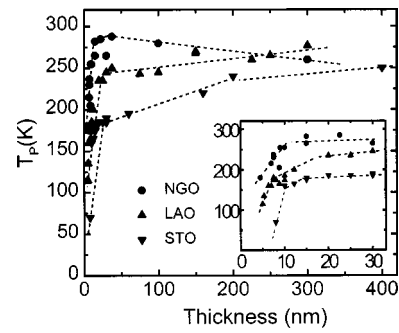


FIG. 5. Thickness dependence of  $T_p$  of the PSMO films grown on LAO ( $\blacktriangle$ ), NGO ( $\bullet$ ), and STO ( $\blacktriangledown$ ) substrates, respectively. Inset highlights the small thickness range. Dashed lines are guide to the eyes.

#### IV. THICKNESS DEPENDENCE OF $T_p$

One of the characteristic features of doped manganites is the occurrence of a resistive transition at  $T_p$  (see inset of Fig. 6) from a high temperature insulating state to a low temperature metallic state, which is close to  $T_C$ . Lattice distortion can clearly influence  $T_p$  (or  $T_C$ ). By examining more than 60 PSMO samples prepared under the same conditions but on different substrates, we have found a systematic thickness dependence of  $T_p$  for films with different strains. At the same thickness, the resistivity of the PSMO/STO film is always higher than those on the other two types of substrate. Concurrently, the  $T_p$  of the PSMO/STO film is the lowest among the three types of samples. Figure 5 shows the dependence of  $T_p$  on  $t$  for the different substrates. The inset highlights the same plot for the small film thickness. This figure has several noticeable features. First, there are two distinguishable thickness ranges in which the  $T_p$  exhibits different  $t$  dependence. For  $t < 20$  nm,  $T_p$  drops sharply with decreasing  $t$  for all three types of films. For  $t > 20$  nm,  $T_p$  shows weak  $t$  dependence. Second, in the range of  $t > 50$  nm, the  $T_p$  of the PSMO/LAO and the PSMO/STO films increases slightly with  $t$ , whereas that of the PSMO/NGO films decreases slightly. Third, the  $T_p$  values of the PSMO/NGO films are the highest and those of the PSMO/STO films are the lowest over the entire thickness range studied.

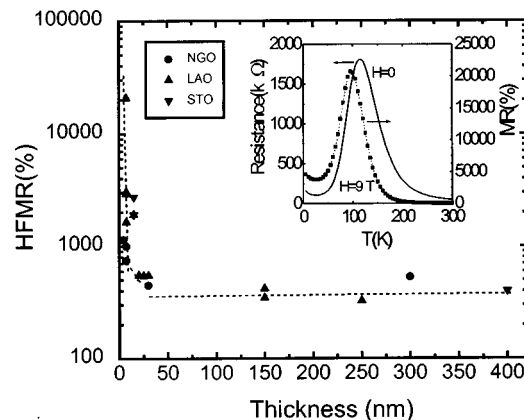


FIG. 6. HFMR as a function of the film thickness for the PSMO films grown on different substrates. Dashed line is guide to the eyes. Inset shows the  $R(T)$  ( $H=0$ ) and the HFMR( $T$ ) ( $H=9T$ ) of a 7.5 nm thick PSMO/LAO film.

## V. MAGNETORESISTANCE

The magnetoresistive effect of the PSMO films is closely related to the zero field transport properties and is very sensitive to strain. We have reported previously that anomalous LFMR properties were observed in the strained films.<sup>10,11</sup> The HFMR, defined as  $-\left[\frac{R(H)-R(0)}{R(H)}\right]$  at  $H=9$  T is plotted as a function of  $t$  in Fig. 6. The inset shows the zero field resistance and the HFMR versus temperature curves of the same sample. Typically, the HFMR– $T$  curve shows a peak at a temperature 10–20 K below  $T_p$ . This behavior has been observed in almost all of our PSMO films regardless of the thickness and the substrate. However, the maximum HFMR value depends on the thickness of the sample. It is in the order of 1000% for films thicker than 20 nm, and is as high as 20 000% for films thinner than 15 nm. The HFMR is almost constant for  $t > 20$  nm and increases sharply with decreasing  $t$  when  $t < 20$  nm. In general, higher HFMR tends to occur in samples with lower  $T_p$ , which is similar to the results in the bulk samples.<sup>13</sup> In addition, the HFMR ratio of the nonstrained PSMO/NGO samples is lower than the highly strained PSMO/LAO and PSMO/STO samples. The HFMR increases monotonously with decreasing thickness in our samples down to 3–5 nm, which is the thickness limit we can still obtain metallic samples. These results differ from those reported in Ref. 9, where a MR maximum was reported at a thickness of about 10 nm.

## VI. DISCUSSION

### A. Thickness dependence of $T_p$

As shown in Fig. 5, for films with  $t > 20$  nm, the  $T_p$  of strained PSMO/LAO and PSMO/STO films show stronger thickness dependence than the nearly strain-free PSMO/NGO films. The result is consistent with the fact that the lattice parameters of the strained films are thickness dependent while in nearly strain-free samples it is thickness independent (Fig. 4). This shows that the  $T_p$  is closely related to strain. However, although the magnitude of the lattice distortion (and hence the strain) in the PSMO/LAO films is larger than the PSMO/STO films, their  $T_p$ s are higher instead of lower. In order to explain this result, one must consider the crystal symmetry difference induced by different strains. Recently, Millis *et al.*<sup>7</sup> asserted that the strain effect on  $T_C$  in a manganite thin film is attributed to two parts: The uniform bulk strain,  $\epsilon_B$ , and the J–T strain,  $\epsilon^*$ . The  $T_C$  can be expressed as

$$T_C(\epsilon) = T_C(\epsilon=0) \left(1 - \alpha \epsilon_B - \frac{1}{2} \Delta \epsilon^{*2}\right), \quad (1)$$

where  $\alpha = 1/T_C dT_C/d\epsilon_B$  and  $\Delta = 1/T_C d^2T_C/d^2\epsilon^*$ . The magnitude of  $\alpha$  and  $\Delta$  represents the relative weight of the symmetry-conserving bulk strain and the symmetry-breaking J–T strain, respectively. The second term in Eq. (1) is related to the change of the kinetic energy of the carriers with respect to the strain. Since  $\epsilon_B = \epsilon_{xx} + \epsilon_{yy} + \epsilon_{zz} = 2(1-P)\epsilon_{\parallel} = (1-1/P)\epsilon_{zz}$  ( $P$  is the Poisson ratio) can be either positive or negative depending on the sign of strain and the value of  $P$ , this term can give either a negative or positive contribution to the  $T_C$ . The third term in Eq. (1) is related to the electron localization due to the splitting of the  $e_g$  level

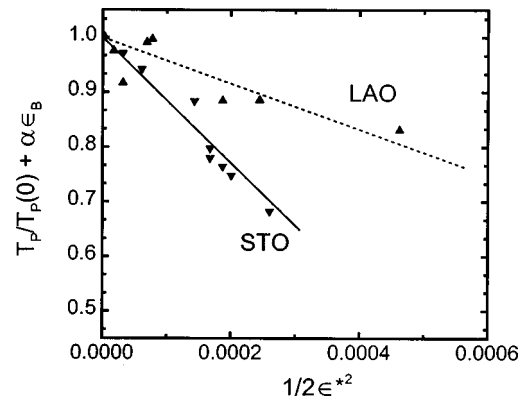


FIG. 7.  $T_p/T_p(0) + \alpha\epsilon_B$  as a function of  $1/2\epsilon^{*2}$  of the PSMO/LAO ( $\blacktriangle$ ) and PSMO/STO ( $\blacktriangledown$ ) films. The dashed and solid lines are linear fit to the data of PSMO/LAO and PSMO/STO samples, respectively. The prefactor  $\Delta$  in Eq. (2) can be obtained directly from the slope of lines.

caused by the static J–T distortion. To calculate the relative contributions of the second and the third terms to  $T_C$ , one needs to know the out-of-plane lattice parameter  $c$  and the in-plane lattice parameter  $a_f$  of the films. We obtained  $P$  from the measured  $c$  and  $a_f$  and found that  $P$  is  $\sim 0.44$ , very close to the reported values of LCMO (0.38) and  $\text{La}_{2/3}\text{Sr}_{1/3}\text{MnO}_3$  (LSMO) (0.42) thin films.<sup>8</sup> With the  $P$  and the  $c$  values from Fig. 3, we found that  $\epsilon_B$  is always negative for PSMO/LAO films and positive for PSMO/STO films. We will use  $T_p$  instead of  $T_C$  for the following discussions since although  $T_C$  and  $T_p$  are different, the difference between them is small.<sup>7,8,14</sup> For the PSMO/LAO samples,  $\epsilon_B$  is negative and hence the bulk compressive strain term in Eq. (1) is positive, a mechanism equivalent to the hydrostatic pressure effect.<sup>5</sup> However, the J–T strain term is always negative. The competition between these two terms results in a moderate reduction of  $T_p$ . For the PSMO/STO samples,  $\epsilon_B$  is positive and both the second and the third terms in Eq. (1) are negative. Therefore,  $T_p$  is reduced further from its bulk value and is lower than that of the PSMO/LAO films at the same thickness. As for the PSMO/NGO samples, both  $\epsilon_B$  and  $\epsilon^*$  are very small, and hence  $T_p$  is relatively close to the bulk value.

Equation (1) can be rewritten as

$$\left[T_C(\epsilon)/T_C(0) + \alpha\epsilon_B\right] = 1 - \frac{1}{2}\Delta\epsilon^{*2}. \quad (2)$$

From the plot  $[T_C(\epsilon)/T_C(0) + \alpha\epsilon_B]$  vs  $1/2\epsilon^{*2}$ , one can obtain the slope  $\Delta$  for a given  $\alpha$ . Figure 7 shows the  $[T_p(\epsilon)/T_p(0) + \alpha\epsilon_B]$  vs  $1/2\epsilon^{*2}$  curves for the PSMO/LAO and PSMO/STO samples. We have taken  $\alpha=11$  from Ref. 7 and  $T_p(0)=280$  from our experiment. Although the data is scattered, it can give a range of the  $\Delta$  value. We determined the  $\Delta$  to be about  $1470 \pm 50$  for the PSMO/STO samples and  $500 \pm 200$  for the PSMO/LAO samples. These values can be compared with that of the LCMO thin films for which  $\Delta \sim 1000$  at  $\alpha=10$  was reported.<sup>7</sup> Obviously, the  $\Delta$  value of the PSMO/STO sample is larger than that of the PSMO/LAO. Since  $\Delta = d^2T_C/d\epsilon^{*2}$ , a larger  $\Delta$  in the tensile strained films represents a stronger J–T effect on the  $T_p(T_C)$ .

The above results lead to an interesting suggestion that the biaxial tensile-strain affects  $T_p$  more than the biaxial compressive-strain in PSMO films with a relatively large

J–T strain contribution. This is also consistent with the results on LCMO thin films by Millis *et al.*,<sup>7</sup> Rao *et al.*,<sup>8</sup> and Koo *et al.*<sup>15</sup> However, Konishi *et al.*<sup>16</sup> and our experiments on the LSMO films<sup>17</sup> do not show the same results. In the LSMO films, the  $T_p(T_c)$  of the compressive-strain LSMO/LAO films is lower than that of the tensile-strain LSMO/STO films for the same film thickness. One possible explanation for this discrepancy is that the lattice mismatch between LSMO (3.88 Å) and LAO (3.79 Å) is too large (–2.4%), and the structural disorder effect becomes dominant over the strain effect. Further experiments are needed to understand the difference of the strain effects in different manganite compounds.

The gradual decrease of  $T_p$  with the increasing  $t$  in the PSMO/NGO films when  $t > 20$  nm is not well understood. It may be due to an increase in structural disorders, such as oxygen vacancies, when the films grow thicker. Since the strain effect in the PSMO/NGO films is negligible, the structural disorder becomes a dominant effect. For the PSMO/LAO and PSMO/STO films, since the strain effects dominate,  $T_p$  increases with  $t$  due to the gradual release of strain.

The above discussion can qualitatively explain the thickness dependence of  $T_p$  for  $t > 20$  nm. However, it is difficult to use the same argument to explain the sharp decrease of  $T_p$  with  $t$  for  $t < 20$  nm. There is no doubt that the strain effect contributes to the reduction of the  $T_p$  because  $T_p$  is always higher for the PSMO/NGO films than that for strained films. But even the strain free PSMO/NGO films show a similar sharp drop in  $T_p$  (see Fig. 5). This may be partially due to the finite size effect on the ferromagnetic ordering and partially due to the structural disorder. Structural disorder and oxygen vacancies exist when large lattice distortions are present. Indeed, we observed broader XRD diffraction peaks in the highly strained ultrathin PSMO/LAO and PSMO/STO films than in the less strained PSMO/NGO samples. The structural disorder can result in spin disorder and enhance the electron scattering and localization. Another important factor which can affect the sharp decrease of  $T_p$  is the surface and interface disorder layer,<sup>18,19</sup> or the “dead layer”<sup>20</sup> as reported recently by several groups. For LSMO films, the estimated dead layer thickness is about 3–5 nm.<sup>20</sup> The effect of the dead layer becomes important when it is comparable to the film thickness because the effective ferromagnetic layer becomes much thinner than the nominal thickness.

## B. MR effect

As shown in Sec. V, for  $t > 20$  nm the HFMR effect is smaller than those for  $t < 20$  nm, and it is almost thickness independent. Furthermore, the HFMR (as well as the LFMR<sup>11</sup>) properties in the thicker films are not sensitive to the substrate used. In the thickness range of  $t < 20$  nm, the HFMR increases sharply with decreasing  $T$  accompanied by a sharp decrease of  $T_p$ . There are several possible explanations for the sharp increase of HFMR with decreasing film thickness. First, the J–T effect induced by the lattice distortions in the highly-strained ultrathin films can enhance the electron localization,<sup>13</sup> resulting in a highly resistive state. By applying a high magnetic field, the electrons delocalize as

the magnetization increases and hence the resistance is reduced. However, the J–T effect is not the only possible reason for the enhanced HFMR at a reduced film thickness, because the PSMO/NGO film also shows an increase in HFMR with decreasing  $t$ . The structural disorder and surface spin disorder effects may become significant as the film thickness is reduced. Indeed, several groups have recently reported an enhanced MR effect<sup>19,21,22</sup> in manganite films and bulk materials by introducing structural and spin disorder. The disorder can result in a reduced mobility of the condition electrons and enhance resistivity. When a high magnetic field is applied, the proportion of the parallel-aligned spins is increased. Therefore conduction is enhanced through the DE process, resulting in a large negative MR.

It should be noted that the thickness dependences of  $T_p$ , LFMR, and HFMR all show a critical thickness at about 15–20 nm in our PSMO films. The physical meaning of this critical thickness is not yet understood. Sun *et al.*<sup>20</sup> have recently shown that there exists a “dead layer” in the CMR films. They attributed the dead layer to the origin of the measured anomalous low-field MR of ultrathin LSMO films. However, the critical thickness (15–20 nm) we observed in the PSMO films is much larger than the reported dead layer thickness (3–5 nm<sup>20</sup>) and our estimated dead layer thickness (<5 nm) from the thickness dependence of the resistivity. Therefore, the critical thickness we observed must have a different origin from the dead layer. In addition, Sun *et al.*<sup>20</sup> showed that the MR (at 3 kOe) of the ultrathin LSMO films exhibits different temperature dependence than the thick films. Their maximum MR temperature is well below  $T_p$  for films thinner than a few nanometers (about the thickness of the dead layer). We have shown previously that the LFMR peak in our strained ultrathin PSMO/LAO films is well below  $T_p$ . However, the HFMR peak in our samples is still very close to  $T_p$  (about 10 K lower than  $T_p$ ) as in bulk samples, even for samples as thin as 5 nm.

## VII. SUMMARY

In summary, by growing PSMO films on different substrates and varying the film thickness, we have systematically examined different strain effects on the magnetotransport properties of the PSMO films. We have found that the  $T_p$  of the PSMO films is suppressed and the MR effects enhanced by strain-induced lattice distortions. The thickness dependence of  $T_p$  and HFMR show evidence for the J–T effect in the strained films. Furthermore, the  $T_p$  of the tensile-strain PSMO films is lower and more sensitive to the strain than the compressive-strain films. The structural defects and the surface spin disorder effects can also contribute to the change of  $T_p$  and the MR effects in the ultrathin films.

## ACKNOWLEDGMENT

The authors thank X. X. Xi, M. Rubinstein, and M. S. Rzchowski for their valuable discussions and T. E. Mallouk for help with the x-ray diffraction. This work is partially supported by NSF Grant Nos. DMR-9876266, DMR-9972973, and the Petroleum Research Fund.

- <sup>1</sup>R. Von Helmlont *et al.*, Phys. Rev. Lett. **71**, 2331 (1993); K. Charhara *et al.*, Appl. Phys. Lett. **63**, 1990 (1993).
- <sup>2</sup>C. Zener, Phys. Rev. **82**, 403 (1951); P. W. Anderson and H. Hasegawa, Phys. Rev. **100**, 675 (1955); P. G. deGennes, Phys. Rev. **118**, 141 (1960).
- <sup>3</sup>A. J. Millis, P. B. Littlewood, and B. I. Shraiman, Phys. Rev. Lett. **74**, 5144 (1995); A. J. Millis, B. I. Shraiman, and R. Mueller, *ibid.* **77**, 175 (1996); A. J. Millis, Nature (London) **392**, 147 (1998).
- <sup>4</sup>H. Roeder, J. Zhang, and A. R. Bishop, Phys. Rev. Lett. **76**, 1356 (1996).
- <sup>5</sup>J.-S. Zhou, J. B. Goodenough, A. Asamitsu, and Y. Tokura, Phys. Rev. Lett. **79**, 3234 (1997).
- <sup>6</sup>D. Louca and T. Egami, J. Appl. Phys. **81**, 5484 (1997).
- <sup>7</sup>A. J. Millis, T. Darling, and A. Migliori, J. Appl. Phys. **83**, 1588 (1998); A. J. Millis, A. Goyal, M. Rajeswari, K. Ghosh, R. Shreekala, R. L. Greene, R. Ramesh, and T. Venkatesan (unpublished).
- <sup>8</sup>R. A. Rao, D. Lavric, T. K. Nath, C. B. Eom, L. Wu, and F. Tsui, Appl. Phys. Lett. **73**, 3294 (1998).
- <sup>9</sup>S. Jin, T. H. Tiefel, M. McCormack, H. M. O'Bryan, L. H. Chen, and D. Schurig, Appl. Phys. Lett. **67**, 557 (1995).
- <sup>10</sup>H. S. Wang and Qi Li, Appl. Phys. Lett. **73**, 2360 (1998).
- <sup>11</sup>H. S. Wang, Qi Li, Kai Liu, and C. L. Chien, Appl. Phys. Lett. **74**, 2212 (1999).
- <sup>12</sup>K. Knizek, Z. Jirak, E. Pollert, F. Zounova, and S. Vratislav, J. Solid State Chem. **100**, 292 (1992).
- <sup>13</sup>C. N. R. Rao and A. K. Raychaudhuri, in *Colossal Magnetoresistance, Charge Ordering and Related Properties of Manganese Oxides*, edited by C. N. R. Rao and B. Raveau (World Scientific, Singapore, 1998), Chap. 1.
- <sup>14</sup>F. M. Araujo-Moreira, M. Rajeswari, A. Goyal, K. Ghosh, V. Smolyaninova, T. Venkatesan, C. J. Lobb, and R. L. Greene, Appl. Phys. Lett. **73**, 3456 (1998).
- <sup>15</sup>T. Y. Koo, S. H. Park, K.-B. Lee, and Y. H. Jeong, Appl. Phys. Lett. **71**, 977 (1997).
- <sup>16</sup>Y. Konish, M. Kasai, M. Isumi, M. Kawasaki, and Y. Tokura, Mater. Sci. Eng., B **56**, 158 (1998).
- <sup>17</sup>Y. F. Hu, H. S. Wang, E. Wertz, and Qi Li (unpublished).
- <sup>18</sup>J.-H. Park, E. Vescovo, H.-J. Kim, C. Kwon, R. Ramesh, and T. Venkatesan, Phys. Rev. Lett. **81**, 1953 (1998).
- <sup>19</sup>J. Fontcuberta, L. Balcells, B. Martinez, and X. Obradors, in *Nano-Crystalline and Thin Film Magnetic Oxides*, edited by I. Nedkov and M. Ausloos (Kluwer, Dordrecht, 1999), p. 105.
- <sup>20</sup>J. Z. Sun, D. W. Abraham, R. A. Rao, and C. B. Eom, Appl. Phys. Lett. **74**, 3017 (1999).
- <sup>21</sup>E. S. Gillman, M. Li, and K.-H. Dahmen, J. Appl. Phys. **84**, 6217 (1998).
- <sup>22</sup>S. B. Ogale *et al.*, J. Appl. Phys. **84**, 6255 (1998).